APPEARANCE OF HIGH SUBMERGED CAVITATING JET: THE CAVITATION PHENOMENON AND SONO-LUMINESCENCE

by

Ezddin HUTLI [a]*, Omer ALTEASH [a], Mostafa BEN RAGHISA [a], Miloš S. NEDELJKOVIĆ [a], and Vojislav ILIĆ [b]

[a] Faculty of Mechanical Engineering, University of Belgrade, Belgrade, Serbia
[b] School of Engineering, University of Western Sydney, Western Sydney, Australia

Original scientific paper
DOI: 10.2298/TSCI120925046H

In order to study jet structure and behaviour of cloud cavitation within time and space, visualization of highly submerged cavitating water jet has been done using Stanford Optics 4 Quick 05 equipment, through endoscopes and other lenses with Drello3244 and Strobex Flash Chadwick as flashlight stroboscope. This included obligatory synchronization with several types of techniques and lenses. Images of the flow regime have been taken, allowing calculation of the non-dimensional cavitation cloud length under working conditions. Consequently a certain correlation has been proposed. The influencing parameters, such as; injection pressure, downstream pressure and cavitation number were experimentally proved to be very significant. The recordings of sono-luminescence phenomenon proved the collapsing of bubbles everywhere along the jet trajectory. In addition, the effect of temperature on sono-luminescence recordings was also a point of investigation.

Key words: *nozzle, cavitating jet, cavitation, time-synchronization, sono-luminescence, cloud length, jet dynamic power*

Introduction

Over the past few years, cavitating fluid jets have received considerable attention, primarily with laboratory experiments. If the unsteady behaviour and the jet structure are clarified in detail, as may be expected, the jet working capacity can be drastically improved [1, 2]. Recently, the cavitating jet is used in many fields such as cleaning paint and rust from metal surfaces, underwater removal of marine fouling, removing of high explosives from munitions, as well as augmenting the action of deep-hole mechanical drilling for petroleum or geothermal energy sources. It is also widely used in cutting, penning, and flushing. The cavitation clouds produced by cavitating jet always behave stochastically, both in time and space, with a very rapid change within seconds [1-7]. In cavitating jets, a small vortex cavitation (initiated in the low-pressure region of the vortex core, which occurs in the shear layer around a high-speed water jet) and the vortex cavitation combine together to form a big cavitation cloud. Cloud shedding is a periodical phenomenon with a frequency of the order of several kHz [5, 8-10]. When the cloud impinges on a surface, a ring vortex cavitation appears. At bubble collapse, a part of the ring forms an erosive vortex cavitation. Shock waves and micro jets are produced at the collapse, which cause a high impact force (≥1500 MPa). In order to obtain a powerful impact, it is necessary to produce such erosive vortex cavitations at a high-efficiency [11-16]. Many param-

* Correspnding author; e-mail: ezddinhutli@yahoo.com

eters have an influence on the performance of cavitating jets (strength of cavitation) such as: hydrodynamic conditions, geometrical conditions (nozzle, test chamber and the target), and fluid properties and its conditions [1, 16]. If a relation between the cavitation intensity in a cavitating jet and the related parameters would be investigated precisely, the key parameter for the prediction of the cavitation behaviour and the side effects such as cavitation erosion, vibration, noise, *etc*. could be clarified [11-17]. As an example it was found that, from the point view of erosion, the behaviour of severely erosive cavitation depends on the pressure gradient in the jet nozzle, the jet geometry and the material of the subject [18-20].

In this paper the visualization of high velocity submerged cavitating water jet at certain hydrodynamic conditions using a 4-Quik-05 camera with several types of lenses is presented and in addition the sono-luminescence phenomenon is also discussed.

Error analysis of the measured quantities (experimental uncertainty)

All the apparatuses in the facility were calibrated in order to obtain results with a high accuracy. The pressure transducers used to measure the upstream and downstream pressure were calibrated precisely with a reference pressure transducer HUBER of high precision, then the flow rates for different nozzle diameters and different directions of flow were measured precisely in order to obtain the constant K in different cases for the calculation of the exit jet velocity (reference velocity). This velocity is used in cavitation number calculation ($\sigma = (P_{\text{ref.}} - P_v)/0.5\,\rho u_{\text{ref.}}^2$), where $p_v(T)$ [bar] is the saturation (vapour) pressure, ρ – the fluid density, $p_{\text{ref.}}$ – the reference pressure (P_2), and u_{ref} – the reference speed (V_J). Reference exit velocities (V_J) during cavitation are based on the single phase flow. For the same mass flow rate, the actual flow velocity will be higher than given (two phase flow). The upstream pressure (P_1) and downstream pressure (P_2) were measured at the inlet and outlet of the test chamber, respectively. The pressure transducers were calibrated by the manufacturer and accuracy certificates were issued for a maximum error of +0.2/–0.21%FS. As the flow rate was determined using P_1 and P_2 values from previous nozzle calibration, its determination uncertainty is also of the order of +/–0.3% FS (full scale). The temperature sensors in the test rig were calibrated perfectly by the use of NORMA (digital thermometer) as the reference in the calibration process. The validity of the cooling system was proved by the examined validity of the heat exchanger and the temperature regulator.

Visualization of cavitating jets using 4-Quik-05 camera

The visualization has been done for high submerged cavitating jet created in chamber field with water. Figure 1 shows the schematic diagram of the test chamber and the cavitating jet impinging on the specimen, respectively; more information about cavitating jet generator presented in previous work [21].

The set-up with Stanford optics 4-QUIK-05 equipment through endoscopes with DRELLO 3244 flashlight stroboscope has been used for further visualization analysis. A personal computer equipped with a Matrox video card through a serial port controls the camera. A monitor was connected to the card for the real-time visualization of the results. The 4-Quick-05 camera is a special black-and-white CCD camera with light amplification (ICCD). Its special shutter permits exposure as short as 30 ns. The adjustable gain allows for operations with very low light, but then resolution drops as the gain is increased. Figure 2 shows the scheme of the visualization system. To overcome the time effect, many single shots have been done for the same working conditions and the average was used for further analysis. The synchronization plays important role in overcoming the time effect.

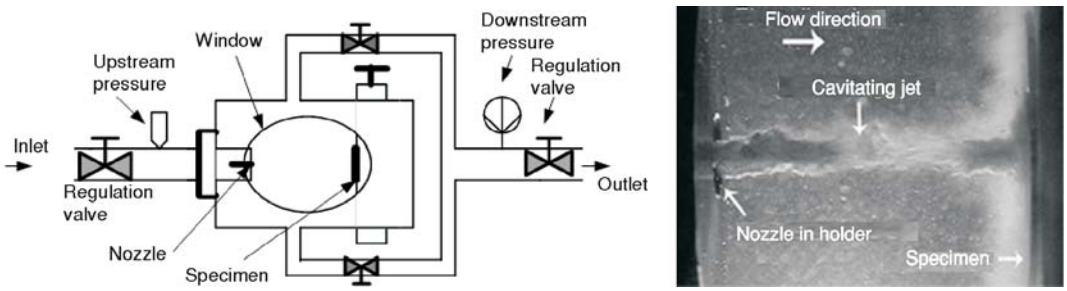

Figure 1. Schematic diagram of test chamber and photo of cavitating jet impinging on the specimen

Synchronization

Because of very rapid changes in the cavitation phenomenon within the order of seconds, and in order to have enough light to illuminate the jet, the shutter and the flash discharge (Drello 3244 or Strobex Flash CHADWICK) were synchronized using a photodiode. The photodiode was connected to an oscilloscope, which generates a TTL signal, used to trigger the camera shutter, fig. 2. A second oscilloscope is used to monitor the synchronization of the flash discharge and the trigger signal.

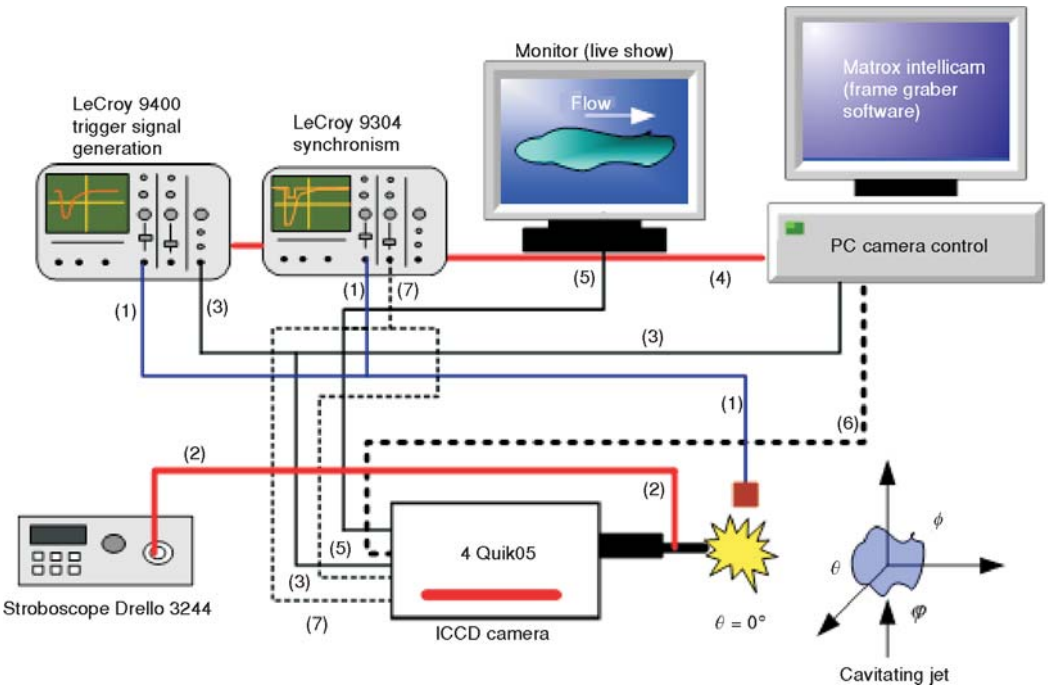

Figure 2. Scheme of the visualization system for the synchronization process; the endoscope is before the test chamber

1 – photodiode signal, 2 – light transmitter, 3 – shuttle trigger, 4 – GPIB connections, 5 – video connection, 6 – RS-232 connection, 7 – synchronization-signal

Visualization of a cavitating jet using a 4-Quik-05 camera with an endoscope

A trial of visualization was done using an endoscope. The endoscope lens and the flashlight lamp were mounted together in a same holder tube, as used in medical investigations. This technique was used for two reasons: first, with the intention to have the flashlight in the same visualization window (in order to have a homogeneous light distribution in the field and thus to illuminate the whole of the jet uniformly), and secondly to approach the test chamber window wall, *i. e.* to be in the nearest position in respect to the jet. The obtained images show that this technique is inappropriate for our case because of the unsatisfactory focus; the lens has to be very near to the subject (of the order of a few millimetres) for getting the optimum results. The images obtained can not be used without magnification, because of inherently poor resolution, *i. e.* the bad quality of the obtained images. So, they are not presented here.

The images in fig. 3 were obtained with the 4-Quik-05 camera. The objective used was Cosmicar television Lens 50 mm with gain of 600 V (in order to achieve a proper exposure) and shutter time of 1 s. Analysis of the group of consecutive images (fig. 3 as an example) reveals that the leading part of the main cavitating jet moves gradually towards the direction of impinging target and then shows a shrinking motion in the jet diameter near the exit of the nozzle. This helps the breaking process in the jet and the peripheral clouds move outward with a shrinking motion and appear to be a string-like vortex cavity with an axis parallel to the target wall surface. The relation between this type of ring-like vortex bubble and the erosion mechanism was presented in previous work [10, 21]. The vanishing of cloud begins to appear near the centre of the large cloud region on the wall and rapidly expands to the whole direction to form an annular cloudy zone. Also the width of the jet is variable and the jet breaking point position is not at the same location in all images because the phenomenon changes within seconds and the used system recorded only one event in each shot. The strong turbulences of the jet are the main reason for the points mentioned earlier. In addition, along the jet path, many bubbles are collapsing, which leads to the change of pressure distribution in the test chamber. Also, many shock waves and micro-jets are created as a result of the bubbles collapsing everywhere along the jet trajectory (fig. 9). In images of fig. 3, some parts of the jet reflected the flashlight, but in general, the upper part of the jet is brighter than the lower part. This is because the flashlight was directed through the upper window. The rings are not the same in size, but this is normal because every picture represents a different instant of the jet's lifetime. As it may be seen in photos, the cavitating jet is changing with time in the order of seconds (this also concluded in [1, 5-10]).

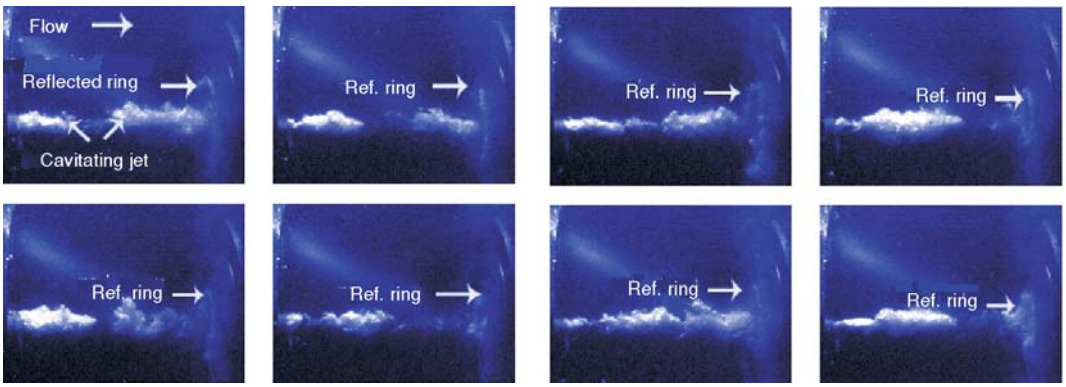

Figure 3. Images of the cavitating jet at; $P_1 = 147$ bar, $P_2 = 0.76$ bar, $V_J = 148$ m/s, $\sigma = 0.0069$, and $T = 18$ °C

Cavitation intensity and the extent of the cavitation cloud

Variations of cavitation intensities and cloud lengths were examined by investigation of influence of some related parameters such as cavitation number, exit jet velocity and jet dynamic power. The power of the jet was changed by adjusting the upstream and downstream pressures (P_1 and P_2, respectively). The valves at the inlet and outlet of the test chamber were used as a tool to change these pressures. The working fluid temperature was constant during the investigation. To describe the power of the jet and fluid energy, the upstream and downstream pressures were measured and the averaged exit velocity (V_J) calculated from the calculated flow rate (Q) (under the assumption of one phase flow). The total power at any point is the summation of static, potential and dynamic power. The dynamic power is assumed to be an effective part of the total power (dynamic is power expressed as $P_{dyn} = 0.5\,\rho V^2 Q$ and is used for creating and driving of the cavitating jets).

In order to have measurable phenomenon, the working condition points were chosen based on previous experience in the work with cavitating jet generator and the help of the cavitation characteristic curves of each nozzle, as shown in the example presented in figs. 4 (divergent and convergent nozzle).

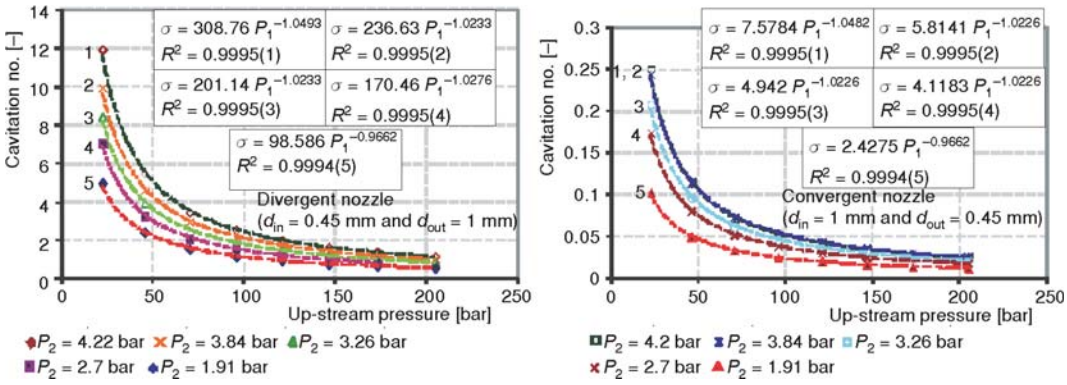

Figure 4. The cavitation characteristic curves used to choose the convenient working points

The cavity length (L_{Cav}) was measured from the obtained images using Photoshop software, then a correction was made according to the real distance between the nozzle lip and target surface (25.67 mm), which was used as the reference. Normalized cavity lengths($L^*_{Cav} = L_{Cav}/d_N$) were determined by post-processing of the acquired images, for the series of 10 frames for each injection pressure (P_1) and each cavitation number (σ), out of L_{Cav} in mm, and d_N (outlet nozzle diameter) in mm. The pressure recorded by the transducer was analysed and the mean cavitation number for each injection pressure calculated. The results are presented in figs. 5 and 6. Figure 5 shows the range of variation of non-dimensional cloud length (jet length) with cavitation num-

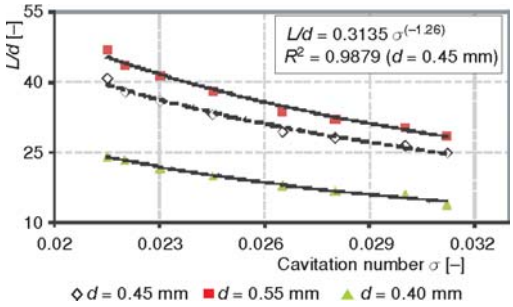

Figure 5. Dependence of non-dimensional cavitating jet length (L_{Cav}/d_N) on cavitation number (σ)

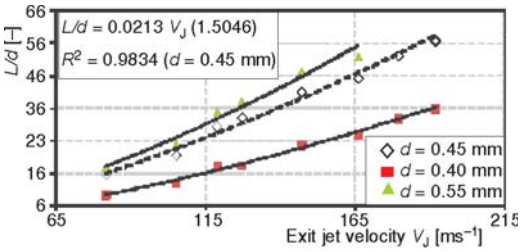

Figure 6. Dependence of non dimensional cavitating jet length (L_{Cav}/d_N) on exit jet velocity (V_J)

ber, and fig. 6 shows the relationship between the cloud length (L_{Cav}/d_N) and the exit-jet velocity (V_J) (may be understood also as a dependence on exit-jet dynamic power ($P_{dyn} = 0.5\,\rho V^2 Q$)). These relationships are of power relationship type, and this type was also presented in [16, 22], but there only between cavitation number and cloud length. In this work the relationship between the cloud length and exit-jet dynamic power is also presented. This relation is more confident because of the real scientific meaning of the dynamic power, while the cavitation number defined in a classical way is not descriptive enough. The correlations in the diagrams are given in eqs. (1) and (2):

$$L/d = 0.313\sigma^{-1.26} \quad \text{(Power relation with } R^2 = 0.9844\text{)} \tag{1}$$

and

$$L/d = 0.0203 V_J^{1.5152} \quad \text{(Power relation with } R^2 = 0.9834\text{)} \tag{2}$$

Equations (1) and (2) (for convergent nozzle $d = 0.45$mm) were determined from the presumed general relation $L/d = A\sigma^{N_1}$ (presented in [16, 21]), and from $L/d = B_1 V_J^{N_2}$, which can be written in the form $L/d = B_2 P_{dyn}^{N_3}$ by substituting the exit jet velocity V_J by the jet dynamic power. ($P_{dyn} = 0.5\rho V^2 Q$). A, B_1, B_2, N_1, N_2, and N_3 are the constants, as represented in figs. 5 and 6, which depend on which parameter will be used (σ, V_J or P_{dyn}). The constants are for the fixed nozzle, since they are very dependent on the nozzle geometry and its dimensions. As mentioned earlier, figs. 5 and 6 was established using the averages of measured 10 frames (photos) for each point.

Visualization of a cavitating jet using a 4-QUIK-05 camera with magnifier lenses

In order to magnify the cavitating jet images to present more information, the objective with magnifier lenses was used. The Navitar Digital Camera Adapter – Navitar's Zoom 6000 system (Navitar 2 × adapter (1-6010) (1-6030) (1-60135) magnifier lenses) was used with a 4-QUIK-05 camera and the flash light Chadwick-Helmuth Strobex (exposure time 30 s). The jet trajectory was divided into three parts (regions) which are overlapping as shown in scheme in fig. 7. Visualization has been done two times: once at $P_2 = 0.77$ bar, $\sigma = 0.0063$ and once at $P_2 = 3.04$ bar, $\sigma = 0.025$. The results are not presented here due to space limitation, but by analysis of the group of consecutive images (even though the resolution was not the best one), it can be easily deducted that all three parts of the jet have dynamic clusters or groups of bubbles, continuously forming and collapsing along the jet length. The jet surface in all images looks highly irregular and uneven, and it is roughened in addition. In some images the flashlight was fully reflected (when the bubbles were spherical), giving rise to clearer images of the jet at $P_2 = 0.77$ bar and $\sigma = 0.0063$ than at other conditions. In addition, we note that the jet width, jet penetration and the number of bubbles increase as P_2 decreases. The size of the bubble cloud can be deduced from the intensity of reflecting light, where the images are brighter at lower values of P_2 (more intensive cavitation). In the case of low P_2, where the jet can reach the target, it can be seen that at the instant of striking, the jet covers the entire target wall with a lot of bubbles which are dis-

tributed over all of the target area. Immediately after the striking, the jet is deflected back and the rings clearly appear in the images. These rings contain thousands of bubbles (fig. 8, last three columns). As mentioned earlier, the produced erosion on the specimen surface has a shape related to the ring shape (reflected ring) [10, 21]. At high P_2 the jet cannot reach the end of the target distance as it is destroyed before the end of trajectory, and therefore the characteristic rings cannot be seen. Also, cloud dynamics (information about strength and compactness of cavitation clouds) can be recognized through image dynamics examination at pixel level (traces brightness of the same cloud with time in consecutive images). Structure analysis within the cloud may be performed too (cloud is not "flat" or "dead" entity, it has its own internal organization governed by the process laying in its background). This fact brings necessity for further image analysis – of the differences in brightness from point to point in the cavitation cloud images. The repetition of the visualizations has been done in order to improve the image quality by playing with the shutter time and gain.

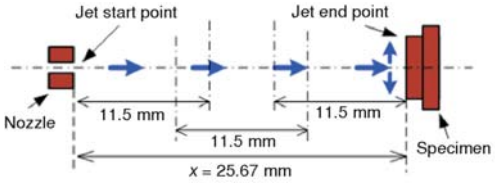

Figure 7. The manner of dividing the cavitating jet during the visualization using a magnifier objective

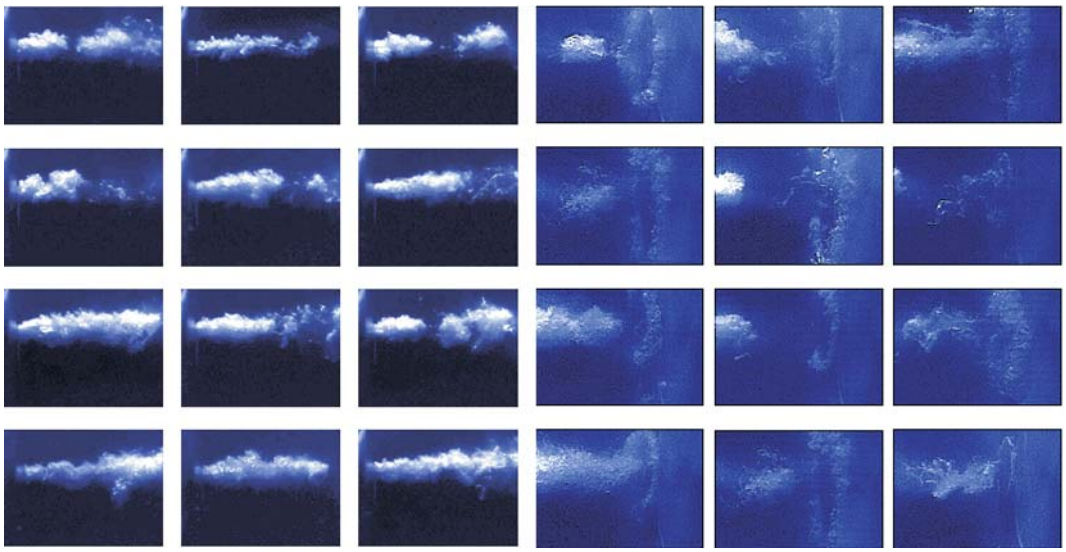

Figure 8. Images of the 1st part of cavitating jet (1st three columns) and of the 3rd part (2nd three columns), magnifier lenses (gain = 600 V, shutter time = 1 μs, P_1 = 164 bar, P_2 = 0.77 bar, V_J =156 m/s, = 0.0063)

Attempt of recording sono-luminescence (SL) phenomenon in cavitating jet

An attempt was also made to record the sono-luminescence (SL) phenomenon associated with the collapse of bubbles in a cavitating jet without adding any kind of additives (noble gases – argon, *etc.*). These attempts were made at different values of cavitation number (σ = = 0.0125, σ = 0.0142, and σ = 0.0207) at constant exit jet-velocity (V_J) and working fluid temperature (T). Figure 9 shows representative frames with SL spots registered by the camera. In

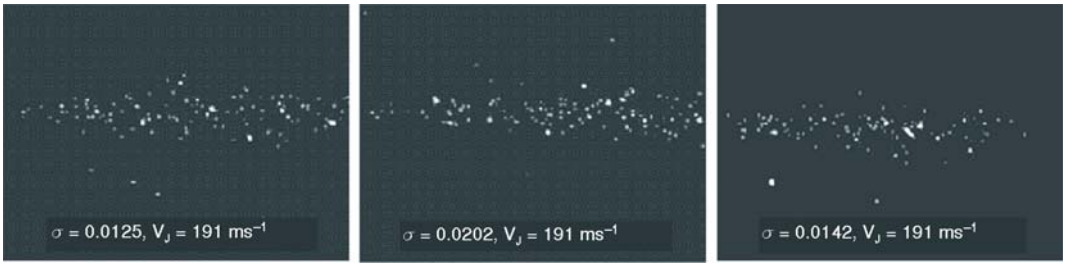

Figure 9. Sono-luminescence phenomenon in a cavitating jet, the flow from left to right (P_1 = 213 bar, V_J = 191 m/s, T = 22 °C)

all shots of SL, the image contrast has been dramatically increased for the reasons of clarity. The aim is to show that the cavity bubbles along the jet path collapse anywhere in and around the jet from its starting point until its end. With this technique, it is possible to identify where the preferred collapse points are located, and how the location and density of the SL bubbles changed with input parameters such as the cavitation number or jet velocity. An intensified CCD camera recorded the light emission simultaneously. The intensified camera (4-QUIK-05) had a standard video output, which could be set to interlaced or non-interlaced mode. The MCP intensifier had a maximum gain of more than 10,000, which was sufficient to ensure that a recorded photon "spot" would have a pixel brightness ten units above the noise level in the CCD. The noise level in the CCD typically did not extend above 29 on a scale of 255 brightness levels (the noise level is determined from the image histogram taken while the intensifier is operated at zero gain), so all levels below 29 were rejected. The camera output was recorded by frame grabber software (Matrox Intellicam). Due to the small fraction of emitted photons, which were intercepted by the camera positioned at the working distance from a jet, relatively few SL flashes were recorded in a single superimposed frame. Due to the values of cavitation numbers, there is no clear difference in density of SL spots between the first and the second image in fig. 9, but the difference exists for the third one. Not all the images obtained by the camera were composed of discrete localised spots of light. Occasionally (once in every few seconds) a comparatively large luminous region would appear in a frame, as in the central part of fig. 9. How these events are to be interpreted is unclear. Perhaps the luminous region was too far removed from the focal plane of the camera, or a large cavity or cloud of cavities passed over the SL spot. Another possibility would be that the observed extended luminous regions actually were composed of a large number of individual SL bubbles. The collapse of a cloud of cavitation bubbles, for example, might also give rise to the effects recorded. In fig.10 the results were obtained at different working fluid temperatures (25°, 36°, and 46 °C) and the other parameters were kept fixed. It was just an attempt to investigate the influence of the tempera-

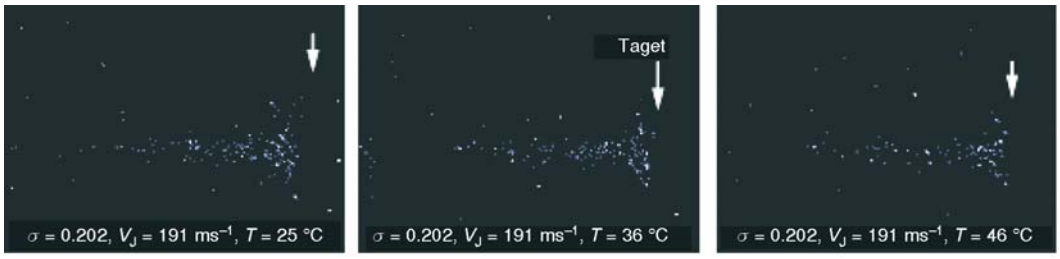

Figure 10. Sono-luminescence phenomenon in a cavitating jet (T = 25, 36, and 46 °C)

ture on the luminescence density and to see if this phenomenon (existence of spherical bubbles) exists or not when the jet is striking the specimen surface. Ten pictures were superimposed over each one, fig. 10. The density of photons was decreased as temperature increased, even though this difference was not appreciable. The influence of temperature on cavitation behaviour has been shown in publications [23, 24]. In addition, there were some spots or photons along the specimen diameter in the form of a ring, *i. e.* the distribution of the bubbles was the same as that of the deflected jet.

Forces acting on a cavitating jet

It is necessary to elucidate the contributions of the acting forces on cavitation cloud (bubble) and how they influence on shape and dynamic manner of cavitation. There are many forces acting on the cloud cavity surface, such as thrust, drag, lift, and gravity force (buoyancy). These are the result of big turbulences in a jet, big differences between the velocities of both the jet and surrounding liquid, and pressure fluctuations inside/around the jet itself. In addition, the variation of the cavity volume within time leads to variation of position of centre of mass of the cavity. The thrust mentioned here is the force exerted by the pump "injection pressure", which pushes the water jet in the forward direction. This thrust is used to create cavitation, but also, some part of it, is used to drive cavitation clouds, and through complex processes its effect will mainly take place at the trailing edge of the cloud. This force is in opposite direction to the drag force, and both of them have big influence on the cavity dynamics and shape characteristics. In general, the total force exerting on a bubble is composed of the contributions of the pressure, gravity, drag, lift, hydrodynamic interaction (hydrodynamic interactions between adjacent bubbles), and virtual mass forces. The drag coefficient is a function of Reynolds number, *i. e.* the properties of fluid flow and bubbles are important parameters for the interaction between cavitation and the acting forces [23-25]. The lift force acting on the cavity bubbles disperses bubbles over the cross-section of the jet path (this mainly happens during or after the break-off fig. 8 first part). This is due to the vorticity, which originates from the shear between the jet and the surrounding liquid. The value of the lift force coefficient is found to be dependent on the Reynolds number and the shear rate [26]. The virtual mass force is the resistance to acceleration, since the fluid accelerates when a bubble accelerates. This force is especially important in the surrounding area at the nozzle exit (bubble generation) [27]. As known, bubbles tend to get deformed when subjected to external fluid forces and fields, until normal and shear stresses balance at the liquid-gas interface (equilibrium state). The actual shape depends on dominating forces, such as surface tension, viscous or inertial force, acting on a cavity bubble [28]. In low viscosity liquids, as water in our case, bubbles (or in fact the clouds) are very irregular and oscillate unsteadily in transition regions between different shapes (spherical, ellipsoidal, distortion parallelogram shape or irregular uniform shape, *etc*. (see the images in figs. 3 and 8).

Conclusion and recommendation

Cavitating jet is a phenomenon changeable with time of the order of μs. The jet appears as white clouds of small bubbles and exhibits a regular frequency of oscillation. The jet behaviour (penetration length, width, *etc*.) depends on the hydrodynamic conditions, such as the cavitation number or P_2 and P_1. When the cavitating jet strikes the wall, the clouds are formed along the surface area producing a jet at the wall and parallel with it. Cavitation rings are produced as result of such an action. In general, diameter of such rings depends on hydrodynamic conditions and nozzle geometry. The collapsing of bubbles could not be registered because of inadequate temporal resolution of the illuminating and recording system, and the huge number

of the bubbles in the cloud cavity (chain production). Observation of the luminescence phenomenon indicates that collapsing of the bubbles takes place everywhere in the jet path. In addition, this proved also the existence of spherical bubbles even for this highly turbulent flow. The kind of visualization system equipment and its resolution is very important to get a good quality of information in the pictures of phenomenon. Given the experimental data obtained in this study, it should be possible to establish a numerical model as the next logical step.

Acknowledgment

The authors would like to thank the Ministry of Education, Science and Technological Development of the Republic of Serbia, for the partial support of this research through the Grant TR35046.

References

[1] Keiichi, S., Yasuhiro, S., Unstable Cavitation Behaviour in a Circular-Cylindrical Orifice Flow, *Trans JSME, ser. B, 45* (2002), 3, pp. 638-645
[2] Soyama, H., *et al*., Observation of the Cavitating Jet in a Narrow Watercourse. Cavitation and Multiphase Flow, *ASME, FED, 194* (1994), pp. 79-82
[3] Conn, A. F., *et al*., Some Industrial Applications of Cavitating Fluid Jets Flow, *Proceedings*, First U. S. Water-Jet Conference, Golden, Col., USA, 1998, pp. 238-253
[4] Fortunato, L., Torrielli, A., Theory of Light Emission In Sono-Luminescence Based upon Transitions in Confined Atoms, *The European Physical Journal D – Atomic, Molecular*, *Optical and Plasma Physics, 33* (2005), 3, pp. 315-463
[5] Soyama, H., High-Speed Observation of a Cavitating Jet in Air,*Trans ASME, Journal of Fluids Engineering, 127* (2005), 4, pp. 1095-1101
[6] Adachi, Y., *et al*., Cavitation-Noise-Characteristics around High Speed Submerged-Water-Jets, *Trans. JSME ser. B, 60* (1994), 571, pp. 730-735
[7] Toyoda, K., *et al*., Visualization of the Vortical Structure of a Circular Jet Excited by Axial and Azimuthal Perturbation, *Journal of Visualization, 2* (1999), 1, pp. 17-24
[8] Soyama, H., *et al*., High-Speed Cavitation-Cloud Observations around High-Speed Submerged Water Jets, *Proceedings*, 2nd International Symposium on Cavitation, Tokyo, Japan, 1994, pp. 225-230
[9] Yamauchi, Y., *et al*., Formation of Process of Vortex Ring Cavitation in High-Speed Submerged Water Jet, *Trans JSME, ser. B, 62* (1996), 593, pp. 72-78
[10] Hutli, E., Nedeljkovic, M., Frequency in Shedding/Discharging Cavitation Clouds Determined by Visualization of a Submerged Cavitating Jet, *Journal of Fluids Engineering, 130* (2008), 2, pp. 561-568
[11] Soyama, H., *et al*., Improvement of Fatigue Strength of Aluminum Alloy by Cavitation Shotless Peening, *Journal of Engineering Materials Technology, 124* (2002), 2, pp. 135-139
[12] Soyama H, Introduction of Compressive Residual Stress Using a Cavitating jet in Air, *Journal of Engineering Materials and Technology, 126* (2006), 1, pp. 123-128
[13] Kwok, C. T., *et al*., Effect of Temperature, pH, and Sulphide on the Cavitation Erosion Behaviour of Super Duplex Stainless Steel, *Wear, 211* (1997), 1, pp. 84-93
[14] Yamaguchi, A., Shimizu, S., Erosion Due to Impingement of Cavitating Jet, *Journal of Engineering Materials and Technology*, *109* (1987), 1, pp. 442-447
[15] Soyama, H., *et al*., Useful Correlations for Cavitating Jets, *Review of High Pressure Science and Technology, 7* (1998), pp. 1456-1458
[16] Yamaguchi, A., Kazama, T., Effects of Configuration of Nozzles, Outlets of Nozzles and Specimens on Erosion Due to Impingement of Cavitating Jet, *Proceedings*, 48th International Exposition for Power Transmission and Technical Conference, Chicago, Ill., USA, 2000, pp. 263-272
[17] Fujikawa, S., *et al*., Cavitation Characteristics of Submerged Water Jet, 3rd International Symposium on Cavitation, Grenoble, France, 1998
[18] Zublin C., Water Jet Cleaning Speeds-Theoretical Determinations, *Proceeding*, 2nd U. S. Water-Jet Conference, Rolla, Mo., USA, 1983, pp. 185-194
[19] Yanaida, K., *et al*., Water Jet Cavitation Performance of Submerged Horn Shaped Nozzles, *Proceedings*, 3rd U. S. Water-Jet Conference, Pittsburgh, Penn., USA, 1985, pp. 266-278

[20] Wolgamott, J., Zink, G., Optimizing Jet Cutting Power for Tube Cleaning, *Proceedings*, 2nd U. S. Water-Jet Conference, Rolla, Mo., USA, 1983, pp. 168-176
[21] Hutli, E., *et al*., Mechanics of Submerged Jet Cavitating Action: Material Properties, Exposure Time and Temperature Effects on Erosion, *Archive of Applied Mechanics, 78* (2008), 5, pp. 329-341
[22] Yamaguchi, A., Shimizu, S., Erosion Due to Impingement of Cavitating Jet, *Transactions of the ASME, 109* (1987), 4, pp. 442-447
[23] Flannigan, D. J., Suslick, K. S., Plasma Formation and Temperature Measurement During Single-Bubble Cavitations, *Nature, 434* (2005), 7029, pp. 52-55
[24] Testud, P., *et al*., Noise Generated by Cavitating Single-hole and Multi-hole Orifices in a Water, *Journal of Fluids and Structures, 23* (2007), 2, pp. 163-189
[25] Magnaudet, J., Legendre, D., The Viscous Drag Force on a Spherical Bubble with a Time-Dependent Radius, *The Physics of Fluids, 10* (1998), 3, pp. 550-554
[26] Bel Fdhila, R., Duineveld, P. C., The Effect of Surfactant on the Rise of a Spherical Bubble at High Reynolds and Peclet Numbers, *Phys. Fluids, 8* (1996), 2, pp. 310-321
[27] Voir, D. J., Michaëlides, E. E., Effect of the History Term on the Motion of Rigid Spheres in a Viscous Fluid, *International Journal of Multiphase Flow, 20* (1994), 3, pp. 547-556
[28] Zapryanov ,Z., Tabakova, S., *Dynamics of Bubbles, Drops, and Rigid Particles*, Kluwer Academic Publishers, Fluid Mechanics and Its Applications, Vol. 50, 1999, ISSN 0926-5112

Paper submitted: September 11, 2012
Paper revised: November 24, 2012
Paper accepted: April 24, 2013